Optimal actuator placement in adaptive optics systems

Altıner, B., Erol, B. & Delibaşı, A.

Optimal Actuator Placement in Adaptive Optics Systems

Berk Altıner[1], Bilal Erol[2] and Akın Delibaşı[3]

Abstract

Adaptive optics systems are powerful tools that are implemented to degrade the effects of wavefront aberrations. In this paper, the optimal actuator placement problem is addressed for the improvement of disturbance attenuation capability of adaptive optics systems due to the fact that actuator placement is directly related to the enhancement of system performance. For this purpose, the linear-quadratic cost function is chosen, so that optimized actuator layouts can be specialized according to the type of wavefront aberrations. It is then considered as a convex optimization problem and the cost function is formulated for the disturbance attenuation case. The success of the presented method is demonstrated by simulation results.

Keywords

adaptive optics, optimal actuator location, optimization, linear quadratic regulator

[1] Department of Control and Automation Engineering, Yıldız Technical University, Istanbul, Turkey.

[2] Department of Aviation Electronics, Yıldız Technical University, Istanbul, Turkey.

[3] School of Mechanical Aerospace and Automotive Engineering, Coventry University, Coventry, United Kingdom.

Corresponding author:

Berk Altıner, Department of Control and Automation Engineering, Yıldız Technical University, Istanbul, Turkey.

Email: berkaltiner@gmail.com

Introduction

Adaptive optics is a growing technology that becomes a necessity in many optical applications such as free-space optical communication, biological imaging, ground-based astronomy and laser beam focusing. Its promising success at correction of wavefront aberrations draws researchers' attention. Adaptive optics systems consist of a deformable mirror (DM), a wavefront sensor (WFS), and a control unit. A schematic representation of adaptive optics systems is shown in Figure 1. Deformable mirrors give the wavefront correction ability to adaptive optics systems and wavefront sensors measure the residual error ($\phi_{res} = \phi_{tur} - \phi_{cor}$) between the distorted wavefront (ϕ_{tur}) and the compensated wavefront (ϕ_{cor}). Next, a control unit determines the shape of deformable mirrors that will compensate for wavefront aberrations.

There are two types of wavefront aberrations: high order aberrations and low order aberrations (Lakshminarayanan and Fleck (2011)). While high order aberrations are widely encountered in applications such as biological imaging, high energy lasers, multifocal systems (Sheppard and Gu (1991), Potsaid et al. (2005)), Hu et al. (2019)), low order aberrations are mostly seen in astronomy applications and they are caused by the atmospheric turbulence and vibrations due to wind effects, coolers, or mechanical components (Powell (2011), Kulcsár et al. (2012a), Correia et al. (2012), Glück et al. (2018)). In the literature, it is shown that adequate modeling of wavefront aberrations provides an efficient way to analyze and eliminate the effects of all types of aberrations. Since the most common aberrations are caused by the atmospheric turbulence, researchers focus on atmospheric turbulence modeling. Andrey Nikolaevich Kolmogorov constructed milestones of atmospheric turbulence modeling. Later, some turbulence spectra are also developed. Among them, two common turbulence spectra called von Karman and Hills-Andrew provide opportunities to observe the effect of inner scale and outer scales which are derived by measurements and observations, in high frequencies.

In order to deal with atmospheric turbulence effects in adaptive optics systems as a control aspect, its temporal behavior is needed. A common way to show the temporal behavior of atmospheric turbulence is using the Taylor hypothesis of frozen turbulence. In this approximation, the atmospheric turbulence is constructed by some of the discrete layers which

have constant wind speed (Conan et al. (1995)). In the control society, some researchers take turbulence as a static gain, neglecting dynamics. Some of them use a simple first-order autoregressive model to express the degraded wavefront by the turbulence. There also exist some works in which the turbulence model is derived by the real-time data (Massioni et al. (2014), Yu and Verhaegen (2018)). The most preferred expression of the turbulence-degraded wavefront is the linear combinations of the orthogonal Zernike polynomials (Conan et al. (1995), Noll (1976), Kulcsár et al. (2012b)). The surface distortions can be expressed as the sum of an infinite number of Zernike polynomials. Fortunately, the first fifteen Zernike polynomial series are sufficient to show 92% of the atmospheric turbulence effect. In (Baudouin et al. (2008)), they construct a state-space representation of atmospheric turbulence with Zernike polynomials, based on the frequency characterization of the atmospheric turbulence and Kolmogorov theory of turbulence.

The major objective of adaptive optics systems is to handle the deformation control, so deformable mirrors are fundamental components of adaptive optics systems. Deformable mirrors are flexible structures. The distributed nature of flexibility makes the dynamic behavior of a system not only dependent on a time variable but also spatial distribution. These kinds of systems belong to the distributed parameter system (DPS) class, and they are governed by partial differential equations (PDE). For such a class of systems, especially in flexible structures, actuator placement is a crucial issue and is the preliminary part of the controller design. The actuator placement problem has been studied since the 1980s. The goal of this subject is to optimize the locations of the actuators for improving the closed-loop performance, ensuring robustness, or minimizing the energy that is consumed to control a system. To optimize the locations of the actuators, an appropriate cost function has to be chosen. In the literature, one of the most common objectives is the maximization of controllability. The maximization of the controllability of a system is achieved by maximizing the minimum eigenvalue of the controllability gramian (Hać and Liu (1993)). Another objective in the actuator placement problem is to eliminate the effects of the initial conditions on system response that is generally handled by the choice of the linear-quadratic (LQ) cost. According to designers' demand, it can be formulated as either the worst-case initial conditions or random initial conditions. For problems governed

by PDEs, an approximation scheme is required to determine the optimal actuator placement, therefore the convergence of the optimal cost is a crucial issue for optimality. In (Morris (2011)), the conditions are provided for the convergence of the LQ optimal actuator placement problem. The robustness against known and unknown disturbances is handled with $\mathcal{H}_2$ and $\mathcal{H}_\infty$ costs respectively (Morris et al. (2015), Kasinathan and Morris (2013)). More detailed discussions for cost functions are presented in survey articles (Frecker (2003), Van De Wal and De Jager (2001), Gupta et al. (2010), Morris and Yang (2015)).

Although the literature abounds with many theoretical and applicable studies on this topic, the actuator placement problem for adaptive optics systems is rarely studied. Energy consumption based optimization is studied via the heuristic way in (Yamaki et al. (2018)). However, the dynamics of the deformable mirror and the aberrations are not taken into consideration. In (Ruppel et al. (2010)), the minimum force modal control is chosen for the performance criteria and it investigates different boundary conditions effect on actuator locations. The optimal sensor placement problem is also studied in (Böhm and Sawodny (2015)) regarding the minimum eigenvalue of the observability gramian as performance indices. To the best of our knowledge, the optimal actuator placement problem which incorporates both the wavefront aberration and the deformable mirror dynamics has not been considered in the literature.

Motivated by the above applications of adaptive optics and since actuator placement is extremely important in the control of flexible structures, the contribution of this paper is to determine the optimal actuator locations for the flexible deformable mirror subject to the linear-quadratic cost. The proposed method provides an efficient way to optimize the actuator locations by focusing on specific optical requirements. From the virtue of our scheme, concentration on specific aberration modes is achieved using weight matrices in the LQ cost. Since the LQ cost relies on actuator locations, that makes the optimization problem defined in a nonconvex cluster. The convexification of the optimal actuator location problem and the solution of this problem through a subgradient algorithm are presented in (Geromel (1989)). However, the results in this work only consider the initial condition effects, and given cost functions in (Geromel (1989)) are not appropriate to cope with the disturbance effects in the adaptive optics control problem. In this context, the proposed optimization
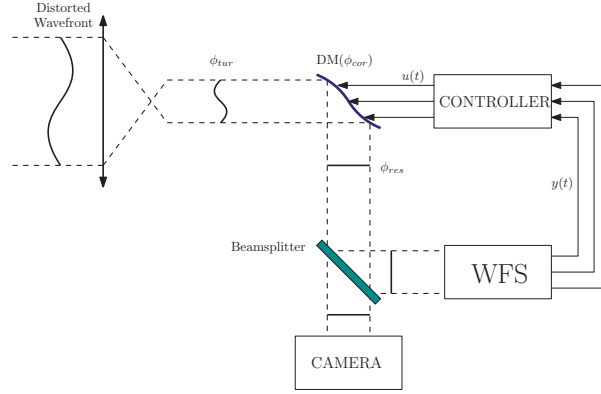
Figure 1. The main structure of adaptive optics system

procedure has to be reformulated for the disturbance attenuation case. The numerical optimization procedure given in (Darivandi et al. (2013)) is adopted to calculate the optimal locations. The closed-loop performance of the system with the linear quadratic regulator (LQR) controller based on the optimal actuator locations is presented.

The rest of the paper is organized as follows. In the modeling section, the mathematical models of the deformable mirror, the wavefront aberrations, and the error dynamics are derived. Then, the LQ actuator location problem is formulated, and the numerical optimization scheme is presented. The numerical results and interpretations are presented in the following section. The final section is devoted to the conclusions.

Notations used throughout this paper are as follows. f' denotes $\frac{\partial f}{\partial x}$, $\dot{f}$ represents $\frac{\partial f}{\partial t}$ and $|| \cdot ||_2$ refers to either the Euclidean vector norm or the induced matrix 2-norm. $A^\dagger$ and A' are pseudoinverse and transpose of a matrix, respectively. $\delta(\cdot)$ is the Kronecker delta operator, $exp(\cdot)$ is the matrix exponential function and $Tr(\cdot)$ is the trace operator. For convenience, the time dependence parameter of the states and the input functions are omitted, i.e ω is for $\omega(t)$.

Mathematical Modeling

In this study, dynamics of wavefront aberrations and the deformable mirror are incorporated into the design procedure. For completeness, the

outputs of both models are taken as Zernike coefficients that are utilized to construct the wavefront error.

Wavefront Aberration Model

The wavefront distortion ($\phi(r, \theta, t)$) caused by the atmospheric turbulence, can be written in polar coordinates (Noll (1976)),

$$\phi(r, \theta, t) = \sum_{j=0}^{\infty} z_{2_j}(t) Z_j(r, \theta), \tag{1}$$

where $z_{2_j}(t)$ is the Zernike coefficients and $Z_j(r, \theta)$ is the Zernike polynomials that are defined on unit circle

$$
\begin{aligned}
Z_{even\ j}(r, \theta) &\triangleq \sqrt{n+1} R_n^m(r) \sqrt{2} cos(m\theta), \quad m \neq 0, \\
Z_{odd\ j}(r, \theta) &\triangleq \sqrt{n+1} R_n^m(r) \sqrt{2} sin(m\theta), \quad m \neq 0, \\
Z_j &\triangleq \sqrt{n+1} R_n^0(r), \quad m = 0
\end{aligned}
\tag{2}
$$

where r is the radial coordinate ranging from 0 to 1 and θ is the azimuthal component ranging from 0 to 2π and

$$R_n^m(r) \triangleq \sum_{k=0}^{\frac{n-m}{2}} \frac{(-1)^k (n-k)!}{k! [\frac{n+m}{2} - k]! [\frac{n-m}{2} - k]!} r^{n-2k}. \tag{3}$$

The Zernike polynomials in Polar Coordinate and its equivalent form in Cartesian Coordinate are given in Table 1 and Figure 2 shows the shape of the Zernike polynomials. A double indexing scheme is used to define the Zernike polynomials, the index n is the radial order and m refers to the azimuthal frequency.

In this study, the first fourteen Zernike polynomials excluding the first mode are considered, so the $N_z = 14$. For the state space representation of the wavefront aberration, the frequency characteristics of turbulence-degraded wavefront given in (Conan et al. (1995)) are exploited. The system matrix of the wavefront aberration contains the low-pass filter structure for the Zernike polynomials

$$H_j(s) = \frac{2\pi f_{c_j}}{s + 2\pi f_{c_j}}, \tag{4}$$

Table 1. The Zernike polynomials in Polar and Cartesian Coordinates

n	m	Polar Coordinate Z_n^m	Cartesian Coordinate Z_n^m
0	0	1	1
1	-1	$2r\sin(\theta)$	y
1	1	$2r\cos(\theta)$	x
2	-2	$r^2\sin(2\theta)$	$2xy$
2	0	$\sqrt{3}(2r^2-1)$	$2x^2+2y^2-1$
2	2	$\sqrt{6}r^2\cos(2\theta)$	x^2-y^2
3	-3	$\sqrt{8}r^3\sin(3\theta)$	$3x^2y-y^3$
3	-1	$\sqrt{8}(3r^3-2r)\sin(\theta)$	$3x^2y+3y^3-2y$
3	1	$\sqrt{8}(3r^3-2r)\cos(\theta)$	$3x^3+3xy^2-2x$
3	3	$\sqrt{8}r^3\cos(3\theta)$	x^3-3xy^2
4	-4	$\sqrt{10}r^4\sin(4\theta)$	$4x^3y-4xy^3$
4	-2	$\sqrt{10}(4r^4-3r^2)\sin(2\theta)$	$8x^3y+8xy^3-6xy$
4	0	$\sqrt{5}(6r^4-6r^2+1)$	$6x^4+12x^2y^2-6x^2+6y^4-6y^2+1$
4	2	$\sqrt{10}(4r^4-3r^2)\cos(2\theta)$	$4x^4-3x^2-4y^4+3y^2$
4	4	$\sqrt{10}r^4\cos(4\theta)$	$x^4-6x^2y^2+y^4$
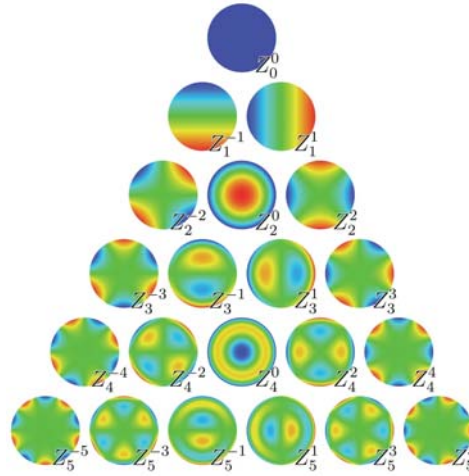
Figure 2. The shape of the first 21 Zernike polynomials

f_{c_j} is the cut-off frequency values of the low-pass filter structures with respect to the Zernike polynomial index n_j and it can be calculated by using the heuristic equation

$$f_{c_j} \cong 0.3(n_j+1)\frac{\mathcal{V}}{\mathcal{D}} \qquad (5)$$

where $\mathcal{V}$ is the atmosphere wind speed and $\mathcal{D}$ is the input lens diameter. The input matrix ($B_2 \in \mathbb{R}^{2N_z \times N_z}$) can be calculated by taking steady state Lyapunov matrix as covariance matrix of Kolmogorov (Baudouin et al. (2008))

$$B_2 B_2' = -(A_2 P_\phi(\infty) + P_\phi(\infty) A_2'), \tag{6}$$

P_ϕ is the covariance matrix which is derived from the Kolmogorov theory on athmospheric turbuence (Baudouin et al. (2008)). The ouput matrix $C_2 \in \mathbb{R}^{2N_z \times 2N_z}$ of the wavefront aberration model is the identity matrix that gives the coefficients of the Zernike polynomials. Finally, the state space representation of the atmoshperic turbulence is obtained as

$$\dot{z}_2 = A_2 z_2 + B_2 \omega \tag{7}$$
$$y_{tur} = C_2 z_2 \tag{8}$$

where $A_2 \in \mathbb{R}^{2N_z \times 2N_z}$ is the matrix with the low-pass filter structure, ω is the noise input signal, z_2 is the state vector which corresponds to the Zernike coefficients and 0 is the zero matrix with appropriate dimension.

Deformable Mirror Model

Deformable mirrors are modeled by using the Kirchhoff plate theory and are governed by biharmonic PDE (Ruppel (2012)). Hence, the mathematical model of the deformable mirror is given by

$$D\left(\frac{\partial^4 w}{\partial x^4} + 2\frac{\partial^4 w}{\partial x^2 \partial y^2} + \frac{\partial^4 w}{\partial y^4}\right) + \rho h \frac{\partial^2 w}{\partial t^2} = u \tag{9}$$

and the flexural rigidity of the deformable mirror

$$D = \frac{Eh^3}{12(1 - \nu^2)} \tag{10}$$

where E, h and ν are the modulus of elasticity, the thickness of the deformable mirror and the Poisson's ratio respectively. In equation (9), ρ is the mass density of the material, w stands for $w(x, y, t)$ and it denotes the deflection of the deformable mirror that depends on spatial variables $x, y \in [0, L]$ and time t. L is the length of edges of the deformable mirror.

Similarly, u in the right hand side of this equation represents the input function $u(x, y, t)$ and it is expressed as

$$u(x, y, t) = \sum_{i=1}^{N_a} b_i(x, y) u_i(t) \tag{11}$$

where $b_i(x, y)$ is the bump function and it is defined as

$$b_i(x, y) = exp\left(-\frac{1}{1 - ((x - x_i)^2 + (y - y_i)^2)}\right) . 1_{\left[\sqrt{(x-x_i)^2+(y-y_i)^2}<\epsilon\right]} \tag{12}$$

and

$$1_{\left[\sqrt{(x-x_i)^2+(y-y_i)^2}<\epsilon\right]} = \begin{cases} 1, & \sqrt{(x - x_i)^2 + (y - y_i)^2} < \epsilon \\ 0, & \text{otherwise} \end{cases} . \tag{13}$$

ϵ is the radius of the actuator influence area and the $\{x_i, y_i\}$ positions denotes the center of this area. N_a is the number of inputs. $u_i(t)$ is the input applied to the deformable mirror from the ith actuator. Deformable mirrors may appear in adaptive optics systems with different boundary conditions such as simply supported end, clamped end or free end. In this study, it is assumed that the deformable mirror is clamped from its edges, so the boundary conditions are

$$w|_{x=0,L} = 0, \ \frac{\partial w}{\partial x}|_{x=0,L} = 0, \tag{14}$$

$$w|_{y=0,L} = 0, \ \frac{\partial w}{\partial y}|_{y=0,L} = 0. \tag{15}$$

In order to approximate the PDE given in equation (9) to the finite number of ODEs, the finite element approximation scheme in (Zienkiewicz et al. (2000)) is used. The finite element discretization yields the finite dimensional approximation of equation (9) in the form of

$$M\ddot{x}_{dm} + B\dot{x}_{dm} + Kx_{dm} = Fu, \tag{16}$$

$$x_{dm} \triangleq \begin{bmatrix} w_i & \theta_{y_i} & \theta_{x_i} \end{bmatrix}', \ i = 1, \ldots, n \tag{17}$$

$$\theta_{y_i} \triangleq \frac{\partial w}{\partial x}, \ \theta_{x_i} \triangleq -\frac{\partial w}{\partial y} \tag{18}$$

where $M, K \in \mathbb{R}^{3n \times 3n}$ are the mass matrix and the stiffness matrix. $F \in \mathbb{R}^{3n \times N_a}$ is the force matrix. Equation (9) has no term for the structural damping of the deformable mirror. For the sake of adding the structural damping to the mathematical model, the Rayleigh damping term which is the $B = \alpha M + \beta K$ is added to the finite dimensional model. α and β are the Rayleigh coefficients. They are chosen based on the following formula

$$\zeta_k = \frac{1}{2w_k} \quad \beta + \left(\frac{w_k}{2}\right)\alpha \tag{19}$$

where w_k is the natural frequencies of the deformable mirror and ζ_k is the damping term that corresponds to the natural frequencies. It is considered that the deformable mirror model has low damping ratio $(0 < \zeta_k < 1)$ at low frequencies and high damping ratio $(\zeta_k > 1)$ at high frequencies. Low frequencies correspond to the frequency band that includes operational region and it is assumed that it varies between $6.24\ rad/s$ and $1872.56\ rad/s$. In the state space form,

$$\dot{z}_1(t) = \underbrace{\begin{bmatrix} 0 & I \\ -M^{-1}K & -M^{-1}B \end{bmatrix}}_{A_1} z_1(t) + \underbrace{\begin{bmatrix} 0 \\ M^{-1}F \end{bmatrix}}_{B_1} u, \tag{20}$$

$$y_{dm}(t) = C_1 z_1(t)$$

where $z_1 = \begin{bmatrix} x_{dm} & \dot{x}_{dm} \end{bmatrix}'$ is the state vector, $A_1 \in \mathbb{R}^{6n \times 6n}$ and $B_1 \in \mathbb{R}^{6n \times N_a}$. The discretized state space model (20) has discrete nodal points on the surface of the deformable mirror. w_i, θ_{y_i} and θ_{x_i} given in (18) are the deflection of the deformable mirror and the phase gradients at i^{th} node. In order to express the output of the deformable mirror in terms of Zernike coordinates, a transformation matrix is required. In (Moser et al. (2015)), the construction of such a transformation matrix using the measured phase gradients is explained. Once the transformation matrix is applied, the output matrix of the deformable mirror model (20) may be defined as $C_1 \in \mathbb{R}^{2N_z \times 6n}$. N_z is the number of Zernike coefficients.

Error Dynamics

The overall system is given in

$$\underbrace{\begin{matrix} \dot{z}_2 \\ \dot{z}_1 \end{matrix}}_{\dot{z}} = \underbrace{\begin{matrix} A_2 & 0 \\ 0 & A_1 \end{matrix}}_{A} \underbrace{\begin{matrix} z_2 \\ z_1 \end{matrix}}_{z} + \underbrace{\begin{matrix} B_2 \\ 0 \end{matrix}}_{B_\omega} \omega + \underbrace{\begin{matrix} 0 \\ B_1 \end{matrix}}_{B_u} u,$$

$$e = \underbrace{\begin{matrix} C_2 & -C_1 \end{matrix}}_{C} \begin{matrix} z_2 \\ z_1 \end{matrix} . \tag{21}$$

In order to express the performance criterion in terms of wavefront error in the design procedure, the error dynamics between the deformable mirror and the wavefront aberration models should be obtained,

$$e = y_{tur} - y_{dm}, \tag{22}$$
$$= C_2 z_2 - C_1 z_1,$$
$$\dot{e} = C_2 \dot{z}_2 - C_1 \dot{z}_1 \tag{23}$$

and

$$\begin{matrix} e \\ \dot{e} \end{matrix} = \underbrace{\begin{matrix} I & 0 & -C_{11} & 0 \\ 0 & I & 0 & -C_{11} \end{matrix}}_{T} \begin{bmatrix} x_{tur} \\ \dot{x}_{tur} \\ x_{dm} \\ \dot{x}_{dm} \end{bmatrix} \tag{24}$$

where C_{11} is the first $N_z \times 3n$ part of the C_1 matrix, 0 and I are the zero and the identity matrix with appropriate dimensions. Then, the coordinate transformation

$$z = T^\dagger \tilde{e} \tag{25}$$
$$\tilde{e} = \begin{matrix} e & \dot{e} \end{matrix}' \tag{26}$$

can be used to convert equation (21) to the error dynamics

$$\dot{\tilde{e}} = \tilde{A}\tilde{e} + \tilde{B}_\omega \omega + \tilde{B}_u u \tag{27}$$

where $\tilde{A} = TAT^\dagger$, $\tilde{B}_\omega = TB_\omega$ and $\tilde{B}_u = TB_u$. The output matrix of the error dynamics stay same with system equation (21).

Linear Quadratic Cost for Optimal Actuator Locations

Consider the LQ optimal control problem and there exists a control signal u minimize the cost

$$J = \lim_{t \to \infty} E[\tilde{e}'Q\tilde{e} + u'Ru] \tag{28}$$

where Q is a positive semi-definite matrix, R is a positive definite matrix and $E[\cdot]$ is the expected value operator. Q and R are weights for the states and the control inputs respectively. For the $u = -G\tilde{e}$, equation (27) is

$$\dot{\tilde{e}} = (\tilde{A} - \tilde{B}_u G)\tilde{e} + \tilde{B}_\omega \omega \qquad (29)$$

and the noise input signal ω in (29) is assumed as the Gaussian white noise with the

$$E[\omega] = 0, \quad E[\omega\omega'] = W\delta(t - \tau) \qquad (30)$$

where W is the covariance matrix. In this manner, the LQ optimal control problem evolves to minimizing the cost against the noise input, so the cost becomes

$$J = Tr\left(PB_\omega W B'_\omega\right) \qquad (31)$$

with the choice of initial condition $\tilde{e}(0) = 0$, P is the solution of the Riccati equation

$$\tilde{A}'P + P\tilde{A} - P\tilde{B}_u R^{-1}\tilde{B}'_u P + Q = 0. \qquad (32)$$

This cost representation is comprised of all actuator locations. However, the goal of this paper is to address the optimal placement for the limited number of actuators. Therefore, the cost function must be reproduced based on alternative actuator layouts. From the standpoint of design, the system matrix $\tilde{B}_u$, defined in equation (27) is dependent on the actuator locations. Then, the previously defined LQ cost given in equation (31) depends also on the actuator location r, and as a matter of this fact the cost function becomes minimization of

$$J = Tr\left(P(r)B_\omega W B'_\omega\right). \qquad (33)$$

Since the decision variable, $P(r)$, is a function of r , the problem is a non-convex optimization problem. To handle this issue, projection is one of the ways. In (Geromel (1989)), it is shown that the projection of the problem onto Π-space and the solution of the Riccati equation onto the parameter space make the problem convex. This elegant assumption is based on the discretization of the solution cluster into a discrete set of possible locations. Here, the set of possible locations is denoted by N_L and it refers to the available actuator locations on the deformable mirror

domain. In this regard, Π-space is spanned by vectors whose elements are consist of 0-1 elements, and $\pi \in \Pi$ is a binary vector with the length of the number of possible actuator locations N_L. The number of ones in π vectors denotes the actuator locations and the zeros are for the nodes where there is no actuator. In other words, if there is one at the jth element of the π vector, it means that there is an actuator at the jth column of the input matrix ($\tilde{B}_u$) of the system. In this context, the new system matrix $\hat{B}_u$ hinges on the actuator locations as follows,

$$\hat{B}_u = \begin{bmatrix} \pi_1 \tilde{B}_{u_1} & \pi_2 \tilde{B}_{u_2} & \cdots & \pi_{N_L} \tilde{B}_{u_{N_L}} \end{bmatrix}$$

and the control weighting matrix R is

$$R = blockdiag(\pi_1 R_1, \ \pi_2 R_2, \ \cdots, \ \pi_{N_L} R_{N_L})$$

.

Therefore, the actuator location problem may be defined as

$$\lim_{t \to \infty} E[(\tilde{e}'Q\tilde{e} + \sum_{j=1}^{N_L} u'_j \pi_j R_j u_j)]$$

$$\text{s.t.} \quad \dot{\tilde{e}} = \tilde{A}\tilde{e} + \tilde{B}_\omega \omega + \sum_{j=1}^{N_L} \pi_j \tilde{B}_{u_j} u_j \qquad (34)$$

$$y = C\tilde{e}.$$

The cost function given in (33) is now expressed as a function of the π vector, so the location dependent cost is

$$\sigma(\pi) \triangleq Tr\left(P(\pi)B_\omega W B'_\omega\right), \qquad (35)$$

and the optimization problem can be summarized as follows

$$\min_{\pi \in \Phi} \sigma(\pi) \qquad (36)$$

$$s.t. \quad \Phi = \{\pi \in \mathbb{R}^{N_L} \ s.t. \pi \in \{0,1\}; \sum_{j=1}^{N_L} \pi_j = N_a\}.$$

and the following theorem shows how to obtain the subgradients for the convexified optimization problem.

Theorem 1. *For the convex set $\Phi_c = \{\pi \in \mathbb{R}^{N_L} \ s.t. \ \pi \geq 0\}$, the objective function $\sigma(\pi) : \Phi_c \to \mathbb{R}$ is convex and for any $\pi_0 \in \Phi_c$ define the following equalities*

$$L_j = B_j R_j^{-1} B_j', \tag{37}$$

$$\mu_j(\pi_0) = Tr\{L_j S(\pi_0)\} \quad j = 1, \ldots, N_L, \tag{38}$$

$$S(\pi_0) = -\frac{1}{2} P(\pi_0) \theta(\pi_0) P(\pi_0) \tag{39}$$

where $\theta(\pi_0)$ is the solution of the Lyapunov equation

$$(A - BK(\pi_0))\theta(\pi_0) + \theta(\pi_0)(A - BK(\pi_0))' + Z = 0, \tag{40}$$

where $Z = B_\omega W B_\omega'$, so a subgradient μ of $\sigma(\pi_0), \pi_0 \in \Phi_c$ can be expressed as

$$\mu(\pi_0) = \ \mu_1(\pi_0) \ldots \mu_{N_L}(\pi_0) \ . \tag{41}$$

To prove the theorem, the primal and the dual versions of the cost function presented in (Geromel (1989)) are exploited. The reason for using the primal and the dual versions is to take advantage of invariance properties of convex sets based on a set of parameters of interest $\Sigma = \{B, C, Q, R\}$. In this context, some definitions that are given in (Geromel (1989)) are revisited for comprehensiveness. First, the quadratic function $H(\pi, x, \lambda)$ is defined to construct the primal and dual versions

$$H(\pi, x, \lambda) \triangleq \frac{1}{2} \ x' \ \ \lambda' \ \begin{bmatrix} Q & A' \\ A & -\sum_{j=1}^{N_L} \pi_j B_j R_j^{-1} B_j' \end{bmatrix} \ \begin{matrix} x \\ \lambda \end{matrix} \ . \tag{42}$$

The quadratic function H is convex with respect to x and it is concave with respect to λ. x and λ can be interpreted as the trajectories of any state space system and they are connected to each other with the relation $\lambda(t) = P(\pi, t)x(t)$. The following sets are defined for exploiting the invariance principle.

$$X(\pi) \triangleq \{x \in \Omega_O \mid \sum_{j=1}^{N_L} \pi_j B_j R_j^{-1} B_j' \lambda = Ax - \dot{x} \quad \text{for some} \quad \lambda \in \Omega_T\} \tag{43}$$

$$D(\pi) \triangleq \{\lambda \in \Omega_T \mid Qx = A'\lambda - \dot{\lambda} \quad \text{for some} \quad x \in \Omega_O\} \tag{44}$$

where Ω_O and Ω_T are the set of differentiable trajectories. Then, the following functional

$$f(\pi, x) \triangleq \max_{\lambda \in \Omega_T} \int_0^t \{H(\pi, x, \lambda) - \lambda' \dot{x}\} \, dt \qquad (45)$$

is convex with respect to x and

$$J(\pi) = \min_{x \in X(\pi)} f(\pi, x). \qquad (46)$$

Similarly,

$$h(\pi, \lambda) \triangleq \min_{x \in \Omega_O} \int_0^t \{H(\pi, x, \lambda) - \lambda' \dot{x}\} \, dt \qquad (47)$$

is concave with respect to λ and

$$J(\pi) = \max_{\lambda \in D(\pi)} h(\pi, \lambda). \qquad (48)$$

(46) and (48) are the primal and dual versions of cost function in (34), then

$$\min_{x \in X(\pi)} f(\pi, x) = J(\pi) = \max_{\lambda \in D(\pi)} h(\pi, \lambda). \qquad (49)$$

In this problem, the decision variable is $\Sigma = \{\pi\}$ and the proof depends on the invariance of the defined sets in (43)-(44) subject to the decision variable. According to the invariance of the sets, the primal or the dual versions of cost are chosen. See (Geromel 1989) for the details. Proof of theorem is given in the Appendix section.

In (Darivandi et al. (2013)), the expansion of Geromel's study (Geromel (1989)) to the multi input case is given and the optimization problem which minimizes the $\sigma(\pi)$ is relaxed as

$$\min_{\pi \in \Phi_c} \max_i \quad \sigma(\pi_i) - \langle \mu(\pi_i), \pi_i \rangle + \langle \mu(\pi_i), \pi \rangle \quad i = 1, \ldots, k \qquad (50)$$

$$s.t. \quad \Phi = \{\pi \in \mathbb{R}^{N_a} \ s.t. \ 0 \leq \pi \leq 1; \sum_{j=1}^{N_L} \pi_j = N_a\}.$$

The algorithm for the solution of the optimization problem (50) is given in Algorithm 1:

Algorithm 1: Linear quadratic optimal actuator location

Input: $\tilde{A}$, $\tilde{B}_\omega$, $\tilde{B}_u$, Q, R, W, N_L, N_a, γ_{min}, k_{max}
Output: $\pi \in \mathbb{R}^{N_L}$
Data: On the convex set Φ_c
```
/* actuator placement   */                      */
```
1 Start with an initial $\pi_0 \in \Phi_c$;
2 Compute $\sigma(\pi_0)$ and $\mu(\pi_0)$ with an initial $\pi_0 \in \Phi_c$;
3 Set $k = 1$ and compute $\mu(\pi_k)$, $\sigma(\pi_k)$ using $\pi_k \in \Phi_c$;
4 **while** $k < k_{max}$ **do**
5   **forall** $i = 0 \cdots k$ **do**
6   **if** $(\sigma_k - \sigma(\pi_i) - \ \mu(\pi_i), \pi - \pi_i \ ) < \gamma_{min}$ **then**
7   terminate
8   compute $\mu(\pi_{k+1})$, $\sigma(\pi_{k+1})$ using $\pi_{k+1} \in \Phi_c$;
9 $k = k + 1$;

Numerical Results

The finite element approximation of order for the deformable mirror is chosen as 9×9 and the possible actuator locations are $N_L = 64$. The discretized mirror surface is depicted in Figure 3. Suppose the number of actuators of which positions are to be optimized is $N_a = 16$. The parameters of the deformable mirror are given in Table 2. The optimization problem given in equation (50) is solved by the Matlab function `fminimax`. In order to calculate the optimal locations, the weighting matrices Q and R are scaled according to the worst possible phase errors, and the maximum value of the control input signal. Then, the concerned error modes are weighted. Although there exist many control techniques based on the Integral Barrier Lyapunov Functionals and neural network-based event trigger control (Li et al. (2016), Liu et al. (2020)), the LQR controller is chosen to show the closed-loop performance of the system. In this way, it is claimed that the LQR controller with optimal location achieves disturbance attenuation better than other possible actuators' layouts. In this context, the oblique astigmatism mode (Z_{-2}^2), the defocus (Z_0^2), the vertical astigmatism (Z_2^2), and the vertical trefoil (Z_3^{-3}) aberration modes are chosen and the white noise disturbance is added to the plant for the atmospheric turbulence effect. The results are

Table 2. Parameter values for the 1 m length square deformable mirror

Parameters	Definition	Value
E	Modulus of Elasticity	63×10^9 Pa
ν	Poisson's ratio	0.2
ρ	Density	2.23×10^3 kg/m^3
h	Thickness	2 mm
α, β	Rayleigh coefficients	0.001
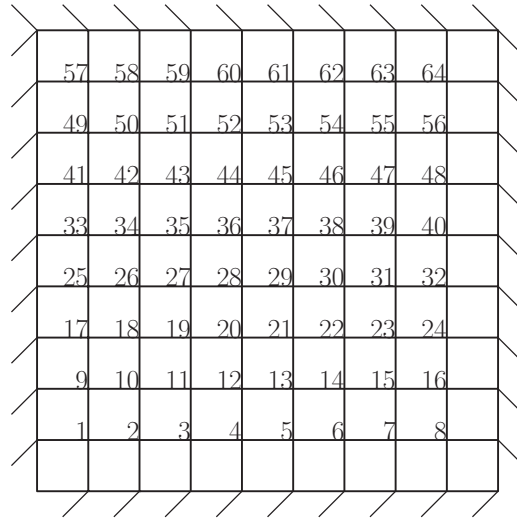
Figure 3. The discretized deformable mirror

given in Table 3-6 and Figure 4-7. $(\dots)^*$ indicates the optimal location and $\tilde{e}_i$ denotes the phase errors for i^{th} Zernike modes.

Table 3 shows the results when the oblique astigmatism mode (Z_{-2}^2) is weighted in the cost function of the location optimization problem. The selected Q and R matrix in the optimization problem are given in (51) and (52). One can see that the optimal actuator location gives the best attenuation performance when it is compared to the other random locations. Figure 4 also shows the performance of LQR controller with the optimal actuator layout.

Table 3. LQR controller performances of the actuator locations for the oblique astigmatism (Z_{-2}^2) error

Actuator Locations	$\|\tilde{e}_3\|_2$	$\sum_{i=1}^{N_a} \|u_i\|_2$	J
(1,8,10,11,14,15,18,23,42,47,50,51,54,55,57,64)*	0.0405	10434	2556.7
(2,5,7,17,29,31,32,33,35,36,38,51,55,58,62,64)	0.0752	10417	3747.7
(4,10,20,25,26,29,32,33,36,40,45,46,47,50,62,63)	0.0559	7906.4	4442.6
(7,10,17,21,26,27,33,34,39,42,46,47,48,52,60,64)	0.0558	9422	3624.8
(3,9,10,11,23,25,33,36,37,41,46,47,59,60,61,62)	0.0482	7848.6	4261
(3,7,8,12,13,14,17,21,32,35,44,48,51,58,60,63)	0.0688	10327	3723.4
(5,9,11,16,18,29,33,37,41,43,46,48,56,58,59,64)	0.0600	91157	3672.8

$$Q_{c_3} = 10^3 \times diag(0.288, 0.098, 1.0390 \times 10^3, 3.0518, 2.4292, \quad (51)$$
$$3.7554, 3.9606, 3.9606, 4.8601, 12.933, 7.1517, 10.978,$$
$$45.028, 31.608, 29.495, 0, 0, 0, 0, 0, 0, 0, 0, 0, 0, 0, 0, 0, 0)$$
$$R_{c_3} = 10^{-4} \times I \quad (52)$$

In Table 4 and Figure 5, the performance of the optimal actuator location and the LQR controller with respect to (53) and (54) are shown for the defocus (Z_0^2) mode. The optimal actuator layout yields the best performance for the disturbance attenuation but consumes high energy, as it can be seen from Table 4. The reason for this result is that when it comes to correct the circular optical deformations such as defocus (Z_0^2) or the coma (Z_3^{-1} and Z_3^1), the structural properties of the deformable mirror, the number of actuators is of significance.

$$Q_{c_4} = 10^3 \times diag(0.288, 0.098, 1.0390 \times 10^3, 3.0518, 2.4292, \quad (53)$$
$$3.7554, 3.9606, 3.9606, 4.8601, 12.933, 7.1517, 10.978,$$
$$45.028, 31.608, 29.495, 0, 0, 0, 0, 0, 0, 0, 0, 0, 0, 0, 0, 0, 0)$$
$$R_{c_4} = 10^{-4} \times I \quad (54)$$

For the vertical astigmatism mode (Z_2^2), the results are given in Table 5 and Figure 6. Q and R matrices used for this case are given in (55) and (56). Similar to the previous cases, the LQR controller with the optimal location minimizes the noise input effect on the interested error mode better than
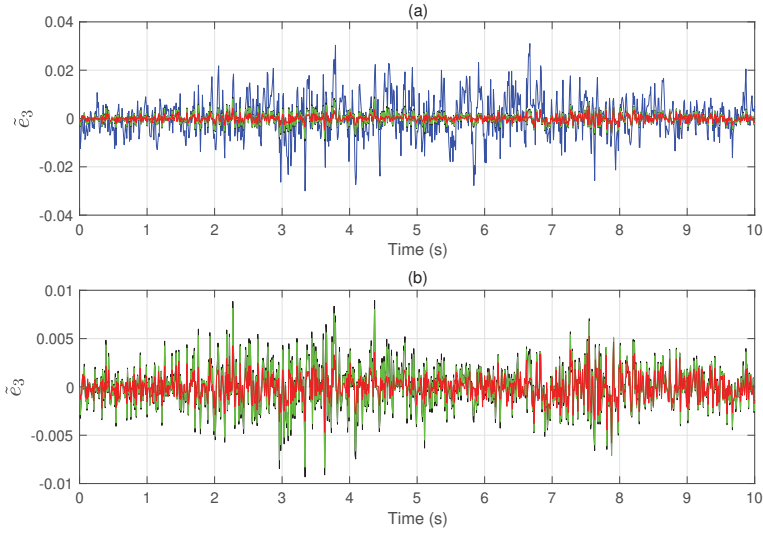
Figure 4. (a) Comparison of LQR controller performance for optimal location (red), random location 1 (black), random location 5 (green) with open loop response (blue). (b) Comparison of LQR controller performance for optimal location (red), random location 1 (black), random location 5 (green)

Table 4. LQR controller performances of the actuator locations for the defocus (Z_0^2) error

Actuator Locations	$||\tilde{e}_4||_2$	$\displaystyle\sum_{i=1}^{N_a} ||u_i||_2$	J
(3,4,5,6,9,16,17,24,41,48,49,56,59,60,61,62)*	0.1222	23508	12688
(2,5,7,17,29,31,32,33,35,36,38,51,55,58,62,64)	0.1381	17604	13090
(4,10,20,25,26,29,32,33,36,40,45,46,47,50,62,63)	0.1379	18246	13087
(7,10,17,21,26,27,33,34,39,42,46,47,48,52,60,64)	0.1386	17521	13156
(3,9,10,11,23,25,33,36,37,41,46,47,59,60,61,62)	0.1300	19898	12986
(3,7,8,12,13,14,17,21,32,35,44,48,51,58,60,63)	0.1368	19127	13073
(5,9,11,16,18,29,33,37,41,43,46,48,56,58,59,64)	0.1364	19013	13063

the controller with random locations. In Figure 6, the effectiveness of the controller with the optimal location is seen clearly.
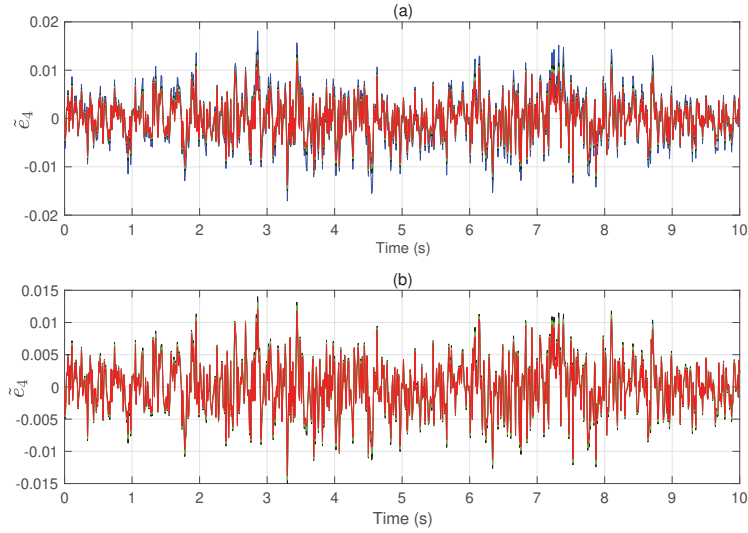
Figure 5. (a) Comparison of LQR controller performance for optimal location (red), random location 6 (black), random location 4 (green) with open loop response (blue). (b) Comparison of LQR controller performance for optimal location (red), random location 6 (black), random location 4 (green)

$$Q_{c_5} = 10^3 \times diag(0.288, 0.098, 1.0390 \times 10^3, 3.0518, 2.4292, \quad (55)$$
$$3.7554, 3.9606, 3.9606, 4.8601, 12.933, 7.1517, 10.978,$$
$$45.028, 31.608, 29.495, 0, 0, 0, 0, 0, 0, 0, 0, 0, 0, 0, 0, 0, 0)$$
$$R_{c_5} = 10^{-4} \times I \quad (56)$$

Finally, the performance of the controller with the optimal actuator location on the vertical trefoil mode is shown in Table 6 and Figure 7. Similar to the previous results, the optimal location for the weighted vertical trefoil mode has the best performance compared to the random locations. Q and R matrices for this mode are given in the equations (57) and (58).

Table 5. LQR controller performances of the actuator locations for the vertical astigmatism (Z_2^2) error

| Actuator Locations	$\lVert \tilde{e}_5 \rVert_2$	$\sum\limits_{i=1}^{N_a} \lVert u_i \rVert_2$	J
(2,7,9,12,13,16,26,31,34,39,49,52,53,56,58,63)*	0.0062	3314.2	1370.1
(2,5,7,17,29,31,32,33,35,36,38,51,55,58,62,64)	0.0123	5008.6	2113.3
(4,10,20,25,26,29,32,33,36,40,45,46,47,50,62,63)	0.0108	3486.7	2703
(7,10,17,21,26,27,33,34,39,42,46,47,48,52,60,64)	0.0070	3051.1	2027.5
(3,9,10,11,23,25,33,36,37,41,46,47,59,60,61,62)	0.0316	11564	2732.7
(3,7,8,12,13,14,17,21,32,35,44,48,51,58,60,63)	0.0091	4290.9	1903.4
(5,9,11,16,18,29,33,37,41,43,46,48,56,58,59,64)	0.0303	12022	2075.7

Figure 6. (a) Comparison of LQR controller performance for optimal location (red), random location 1 (black), random location 6 (green) with open loop response (blue). (b) Comparison of LQR controller performance for optimal location (red), random location 1 (black), random location 6 (green)

$$Q_{c_6} = 10^3 \times diag(0.288, 0.098, 1.0390 \times 10^3, 3.0518, 2.4292, \qquad (57)$$
$$3.7554, 3.9606, 3.9606, 4.8601, 12.933, 7.1517, 10.978,$$
$$45.028, 31.608, 29.495, 0, 0, 0, 0, 0, 0, 0, 0, 0, 0, 0, 0, 0, 0)$$

$$R_{c_6} = 10^{-4} \times I \qquad (58)$$

Table 6. LQR controller performances of the actuator locations for the vertical trefoil (Z_3^{-3}) error

Actuator Locations	$\|\tilde{e}_6\|_2$	$\sum_{i=1}^{N_a}\|u_i\|_2$	J
(3,4,5,6,9,16,17,24,41,48,49,56,59,60,61,62)*	0.0305	16342	3244.7
(2,5,7,17,29,31,32,33,35,36,38,51,55,58,62,64)	0.0546	18076	4576
(4,10,20,25,26,29,32,33,36,40,45,46,47,50,62,63)	0.0428	14098	4687.5
(7,10,17,21,26,27,33,34,39,42,46,47,48,52,60,64)	0.0363	12242	4550
(3,9,10,11,23,25,33,36,37,41,46,47,59,60,61,62)	0.0362	14797	3946.4
(3,7,8,12,13,14,17,21,32,35,44,48,51,58,60,63)	0.0513	17226	4452.6
(5,9,11,16,18,29,33,37,41,43,46,48,56,58,59,64)	0.0341	13785	3965.1
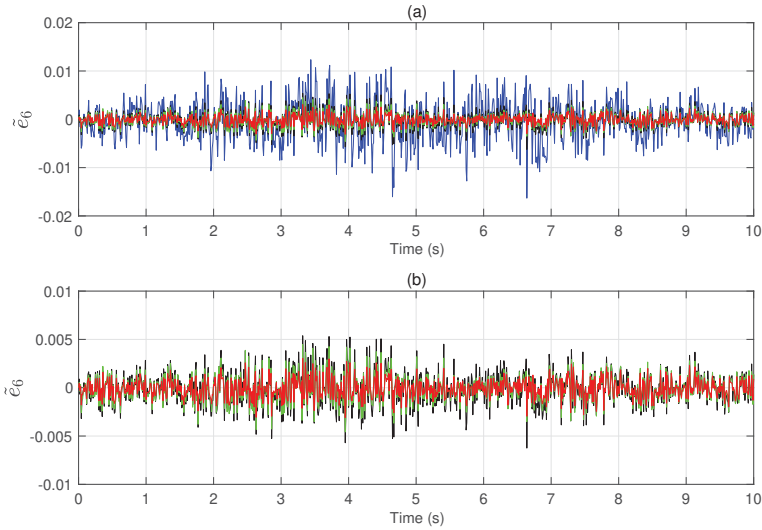
Figure 7. (a) Comparison of LQR controller performance for optimal location (red), random location 1 (black), random location 2 (green) with open loop response (blue). (b) Comparison of LQR controller performance for optimal location (red), random location 1 (black), random location 2 (green)

CONCLUSIONS

In this paper, the optimal actuator placement problem is investigated for adaptive optics systems. To do that, the structural dynamics of the deformable mirror and the dynamics of the wavefront aberrations are considered in the design procedure. Since the adaptive optics control

problem is mainly based on the disturbance attenuation, the cost function is reformulated for this case. Then, the actuator locations for the different aberration modes are optimized by minimizing the LQ cost. The simulation results show that the closed-loop performance of the system with the optimal actuator layouts performs much better than any other random actuator layouts for the concerned optical aberration modes.

Acknowledgements

References

Baudouin L, Prieur C, Guignard F and Arzelier D (2008) Control of adaptive optics system: an $\mathcal{H}_\infty$ approach. *IFAC Proceedings Volumes* 41(2): 13408–13413.

Böhm M and Sawodny O (2015) Optimal sensor placement for modal based estimation of deformable mirror shape. In: *Control Applications (CCA), 2015 IEEE Conference on*. IEEE, pp. 418–423.

Conan JM, Rousset G and Madec PY (1995) Wave-front temporal spectra in high-resolution imaging through turbulence. *JOSA A* 12(7): 1559–1570.

Correia C, Véran JP and Herriot G (2012) Advanced vibration suppression algorithms in adaptive optics systems. *JOSA A* 29(3): 185–194.

Darivandi N, Morris K and Khajepour A (2013) An algorithm for lq optimal actuator location. *Smart materials and structures* 22(3): 035001.

Frecker MI (2003) Recent advances in optimization of smart structures and actuators. *Journal of Intelligent Material Systems and Structures* 14(4-5): 207–216.

Geromel JC (1989) Convex analysis and global optimization of joint actuator location and control problems. *IEEE Transactions on Automatic Control* 34(7): 711–720.

Glück M, Pott JU and Sawodny O (2018) Model predictive control of multi-mirror adaptive optics systems. In: *2018 IEEE Conference on Control Technology and Applications (CCTA)*. IEEE, pp. 909–914.

Gupta V, Sharma M and Thakur N (2010) Optimization criteria for optimal placement of piezoelectric sensors and actuators on a smart structure: a technical review. *Journal of Intelligent Material Systems and Structures* 21(12): 1227–1243.

Hać A and Liu L (1993) Sensor and actuator location in motion control of flexible structures. *Journal of sound and vibration* 167(2): 239–261.

Hu L, Hu S, Gong W and Si K (2019) Learning-based shack-hartmann wavefront sensor for high-order aberration detection. *Optics express* 27(23): 33504–33517.

Kasinathan D and Morris K (2013) $\mathcal{H}_\infty$-optimal actuator location. *IEEE Transactions on Automatic Control* 58(10): 2522–2535.

Kulcsár C, Massioni P, Sivo G and Raynaud HFG (2012a) Vibration mitigation in adaptive optics control. In: *Adaptive Optics Systems III*, volume 8447. International Society for Optics and Photonics, p. 84470Z.

Kulcsár C, Raynaud HF, Petit C and Conan JM (2012b) Minimum variance prediction and control for adaptive optics. *automatica* 48(9): 1939–1954.

Lakshminarayanan V and Fleck A (2011) Zernike polynomials: a guide. *Journal of Modern Optics* 58(7): 545–561.

Li DJ, Li J and Li S (2016) Adaptive control of nonlinear systems with full state constraints using integral barrier lyapunov functionals. *Neurocomputing* 186: 90–96.

Liu L, Liu YJ, Chen A, Tong S and Chen CP (2020) Integral barrier lyapunov function-based adaptive control for switched nonlinear systems. *Science China Information Sciences* 63(3): 1–14.

Massioni P, Raynaud HF, Kulcsár C and Conan JM (2014) An approximation of the riccati equation in large-scale systems with application to adaptive optics. *IEEE transactions on control systems technology* 23(2): 479–487.

Morris K (2011) Linear-quadratic optimal actuator location. *IEEE Transactions on Automatic Control* 56(1): 113–124.

Morris K, Demetriou MA, Yang SD et al. (2015) Using bbh2-control performance metrics for the optimal actuator location of distributed parameter systems. *IEEE Trans. Automat. Contr.* 60(2): 450–462.

Morris K and Yang S (2015) Comparison of actuator placement criteria for control of structures. *Journal of Sound and Vibration* 353: 1–18.

Moser S, Lee P and Podoleanu A (2015) An fpga architecture for extracting real-time zernike coefficients from measured phase gradients. *Measurement Science Review* 15(2): 92–100.

Noll RJ (1976) Zernike polynomials and atmospheric turbulence. *JOsA* 66(3): 207–211.

Potsaid B, Bellouard Y and Wen JT (2005) Adaptive scanning optical microscope (asom): a multidisciplinary optical microscope design for large field of view and high resolution imaging. *Optics Express* 13(17): 6504–6518.

Powell K (2011) Estimating the effects of structural vibration on adaptive optics system performance. *Applied optics* 50(15): 2185–2191.

Ruppel T (2012) Modeling and control of deformable membrane mirrors. In: *Adaptive Optics Progress*. InTech.

Ruppel T, Sawodny O and Osten W (2010) Actuator placement for minimum force modal control of continuous faceplate deformable mirrors. In: *Control Applications (CCA), 2010 IEEE International Conference on*. IEEE, pp. 867–872.

Sheppard CJ and Gu M (1991) Aberration compensation in confocal microscopy. *Applied optics* 30(25): 3563–3568.

Van De Wal M and De Jager B (2001) A review of methods for input/output selection. *Automatica* 37(4): 487–510.

Yamaki Y, Sato Y, Izui K, Yamada T, Nishiwaki S, Hirai Y and Tabata O (2018) A heuristic approach for actuator layout designs in deformable mirror devices based on current value optimization. *Structural and Multidisciplinary Optimization* : 1–12.

Yu C and Verhaegen M (2018) Structured modeling and control of adaptive optics systems. *IEEE Transactions on Control Systems Technology* 26(2): 664–674.

Zienkiewicz OC, Taylor RL and Taylor RL (2000) *The finite element method: solid mechanics*, volume 2. Butterworth-heinemann.

Appendix A

Proof. Following the same idea in (Geromel (1989)), let the optimization problem (34) is solved for $\pi_0 \in \Phi_c$ and (x_0, λ_0) denote the optimal trajectories correspond to $\pi_0 \in \Phi_c$. From theorem,

$$
\begin{aligned}
J(\pi_0) &= \max_{\lambda \in D(\pi)} h(\pi_0, \lambda) \\
&= h(\pi_0, \lambda_0) \\
&= \min_{x \in \Omega_O} \lim_{t \to \infty} E[\{H(\pi_0, x, \lambda_0) - \lambda_0' \dot{x}] \\
&= \lim_{t \to \infty} E[\{H(\pi_0, x_0, \lambda_0) - \lambda_0' \dot{x}_0\}]
\end{aligned}
\tag{59}
$$

and for $\forall \pi \in \Phi$,

$$
\begin{aligned}
J(\pi) &= \max_{\lambda \in D(\pi)} h(\pi, \lambda) \\
&\geq h(\pi, \lambda_0) \\
&= \min_{x \in \Omega_0} \lim_{t \to \infty} E[H(\pi, x, \lambda_0) - \lambda_0' \dot{x}\}].
\end{aligned}
\tag{60}
$$

The quadratic function $H(\pi, x, \lambda_0)$ can be decomposed as

$$
H(\pi, x, \lambda_0) = H(\pi_0, x, \lambda_0) - \frac{1}{2} \sum_{j=1}^{N_L} (\pi_j - \pi_{0j}) \lambda_0' L_j \lambda_0
\tag{61}
$$

and if equation (61) is substituted in (60)

$$J(\pi) \geq \underbrace{\min_{x \in \Omega_O} \lim_{t \to \infty} E[H(\pi_0, x, \lambda_0) - \lambda_0' \dot{x}]}_{J(\pi_0)} \tag{62}$$

$$- \lim_{t \to \infty} E \left[\frac{1}{2} \int_0^t \sum_{j=1}^{N_L} (\pi_j - \pi_{0j}) \lambda_0' L_j \lambda_0 \right]$$

$$J(\pi) \geq J(\pi_0) - \lim_{t \to \infty} E \left[\frac{1}{2} \int_0^t \sum_{j=1}^{N_L} (\pi_j - \pi_{0j}) \lambda_0' L_j \lambda_0 \right]. \tag{63}$$

are obtained. Then, from the relation $\lambda_0(t) = P(\pi_0, t) x_0(t)$ and the solution of (29) with zero initial condition

$$x_0(t) = \int_0^t \exp(A_{cl}(t - \tau)) B_\omega \omega(\tau) d\tau \tag{64}$$

where $A_{cl} \triangleq A - \sum_{j=1}^{N_L} \pi_j \tilde{B}_{u_j} G$, the second term in the right hand side of inequality (63) can be rewritten as follows

$$= \lim_{t \to \infty} E \left[-\frac{1}{2} \int_0^t \sum_{j=1}^{N_L} (\pi_j - \pi_{0j}) \int_0^t \omega(\tau)' B_\omega' \exp(A_{cl}'(t - \tau)) d\tau P(\pi_0, t) L_j P(\pi_0, t) \int_0^t \exp(A_{cl}(t - \varsigma)) B_\omega \omega(\varsigma) d\varsigma \right] \tag{65}$$

Using the properties of the trace operator given in Appendix B, and equation (30)

$$= \lim_{t \to \infty} Tr \left(-\frac{1}{2} \sum_{j=1}^{N_L} (\pi_j - \pi_{0j}) L_j \int_0^t B_\omega' \exp(A_{cl}'(t - \tau)) P(\pi_0, t) \int_0^t E \left[\omega(\tau) \omega'(\varsigma) \right] P(\pi_0, t) \exp(A_{cl}(t - \varsigma)) B_\omega d\varsigma d\tau \right)$$

$$= \lim_{t \to \infty} Tr \left(-\frac{1}{2} \sum_{j=1}^{N_L} (\pi_j - \pi_{0j}) L_j \int_0^t B_\omega' \exp(A_{cl}'(t - \tau)) P(\pi_0, t) \int_0^t W \delta(\tau - \varsigma) P(\pi_0, t) \exp(A_{cl}(\tau - \varsigma)) B_\omega d\varsigma d\tau \right) \tag{66}$$

$$= \lim_{t \to \infty} Tr \left(-\frac{1}{2} \sum_{j=1}^{N_L} (\pi_j - \pi_{0j}) L_j \int_0^t P(\pi_0, t) \exp(A_{cl}(t - \tau)) B_\omega W B_\omega' \exp(A_{cl}'(t - \tau)) P(\pi_0, t) d\tau \right) \tag{67}$$

$$Tr \left(-\frac{1}{2} \sum_{j=1}^{N_L} (\pi_j - \pi_{0j}) L_j P(\pi_0) \theta(\pi_0) P(\pi_0) \right) = Tr \left(\sum_{j=1}^{N_L} (\pi_j - \pi_{0j}) L_j S(\pi_0) \right) \tag{68}$$

where $S(\pi_0) \triangleq -\frac{1}{2}P(\pi_0)\theta(\pi_0)P(\pi_0)$ and $\theta(\pi_0)$ is the solution of

$$(A - BG(\pi_0))\theta(\pi_0) + \theta(\pi_0)(A - BG(\pi_0))' + B'_\omega W B_\omega = 0. \quad (69)$$

Then,

$$\sigma(\pi) \geq \sigma(\pi_0) + Tr \quad S(\pi_0) \sum_{j=1}^{N_L} (\pi_j - \pi_{0j})L_j \quad (70)$$

$$= \sigma(\pi_0) + \sum_{j=1}^{N_a} (\pi_j - \pi_{0j})Tr\left(S(\pi_0)L_j\right) \quad (71)$$

$$= \sigma(\pi_0) + \quad \mu(\pi_0), \pi - \pi_0 \quad (72)$$

and the theorem is proved.

Appendix B

The trace operator $Tr(\cdot)$ satisfies the following equality.

$$x^T x = Tr(x^T x) = Tr(xx^T) \quad (73)$$